An islanded microgrid energy management controller validated by using Hardware-In-the-Loop Emulators

D. Petreus [a], R. Etz [a], T. Patarau [a], M. Cirstea [b]

[a] Technical University of Cluj-Napoca, Faculty of Electronics, Telecommunications and Information Technology, Applied Electronics Department, Memorandumului Street no. 28, Cluj-Napoca, 400114, Romania, tel: +40264202348.

[b] Anglia Ruskin University, Computing and Technology Department, East Road, Cambridge, CB1 1PT, tel. +44-1223-698184

Abstract

A novel microgrid emulator used to test multiple microgrid configurations and energy management control strategies is presented. The system includes Hardware-In-the-Loop (HIL) emulators for geothermal and biogas energy sources. It also includes actual photovoltaic energy together with a lead acid battery bank for storage and it is controlled by a two level control system. The control system consists of a primary level voltage-reactive power and frequency-active power and a secondary level energy management algorithm based on the balance between the power produced by the renewable energy generators, state of charge of the battery bank and the loads. The energy management control strategy is based on cycle-charging the batteries at a reference value in order to efficiently use the available resources. The primary energy source is considered the geothermal energy, while the most cost effective one is the photovoltaic energy. A buffer zone is kept in the battery bank in order to store as much energy produced by the photovoltaic system as possible. The presented microgrid, used for testing the energy management strategies, employs emulators for the geothermal and biogas generators; however, the results are relevant and can be scaled for a real-life microgrid.

Keywords: microgrid, power management, renewable energies, two level control, cycle charge control.

1 Introduction

From the analysis of the Energy Information Administration [1], it results that the world energy consumption increases with 2.3% each year. It is estimated that by 2035 the energy consumption will rise by more than 50% compared to the current situation [1]. Year 2015 was the first year when the amount of energy produced by hydropower stations was overtaken by the energy produced by wind, solar and other renewable energy sources.

According to [2], there are two categories of energy technologies: on one hand the hydro, biomass and geothermal power form the first-generation and on the other hand the solar, wind, bioenergy and photovoltaics form the second generation. Microgrids combine these renewable energy resources and can be viewed as power controllable distributed energy generators. Distributed generators can either act as backup energy sources or as upgrades for the existing grid and can include also conventional internal combustion engines and gas turbines. It should also be mentioned that in many countries isolated communities (more than 20 km from the grid) are not being considered for further extensions of the grid.

An energy system that incorporates more than one energy sources is called a hybrid renewable energy system (HRES). In most cases, using such systems leads to higher reliability and lower operation cost than in the case of using only one energy source.

Optimization applications for HRES which integrate various renewable energy sources in microgrids are present in literature. In [3], a mathematical solution for control management of a hybrid microgrid is presented. Two levels of control can be denominated: a primary control based on droop and a secondary one that eliminates steady state errors or schedules the use of energy resources based on real time and historic data measured from the microgrid. The first level balances the voltage and frequency in the microgrid and the second one reduces the cost of operation and increases the reliability of the microgrid using a planned operating framework [4] and [5]. For the second level control, a central computational unit and measuring devices are used, in most cases with communication capability or methods such as the one presented in [6]. By using an energy management control unit, the intermittent availability of the resources can be partially overcome through predictive techniques. In [7], a smart energy management system tool for microgrid optimization operation is presented. Various studies for hybrid microgrid operational schedule, configurations, control methods and energy management are presented in [8,9].

For an accurate analysis and optimization, a rigorous model for each component in a HRES is needed since without optimal utilization of the energy sources, the cost of a small microgrid is not justified.

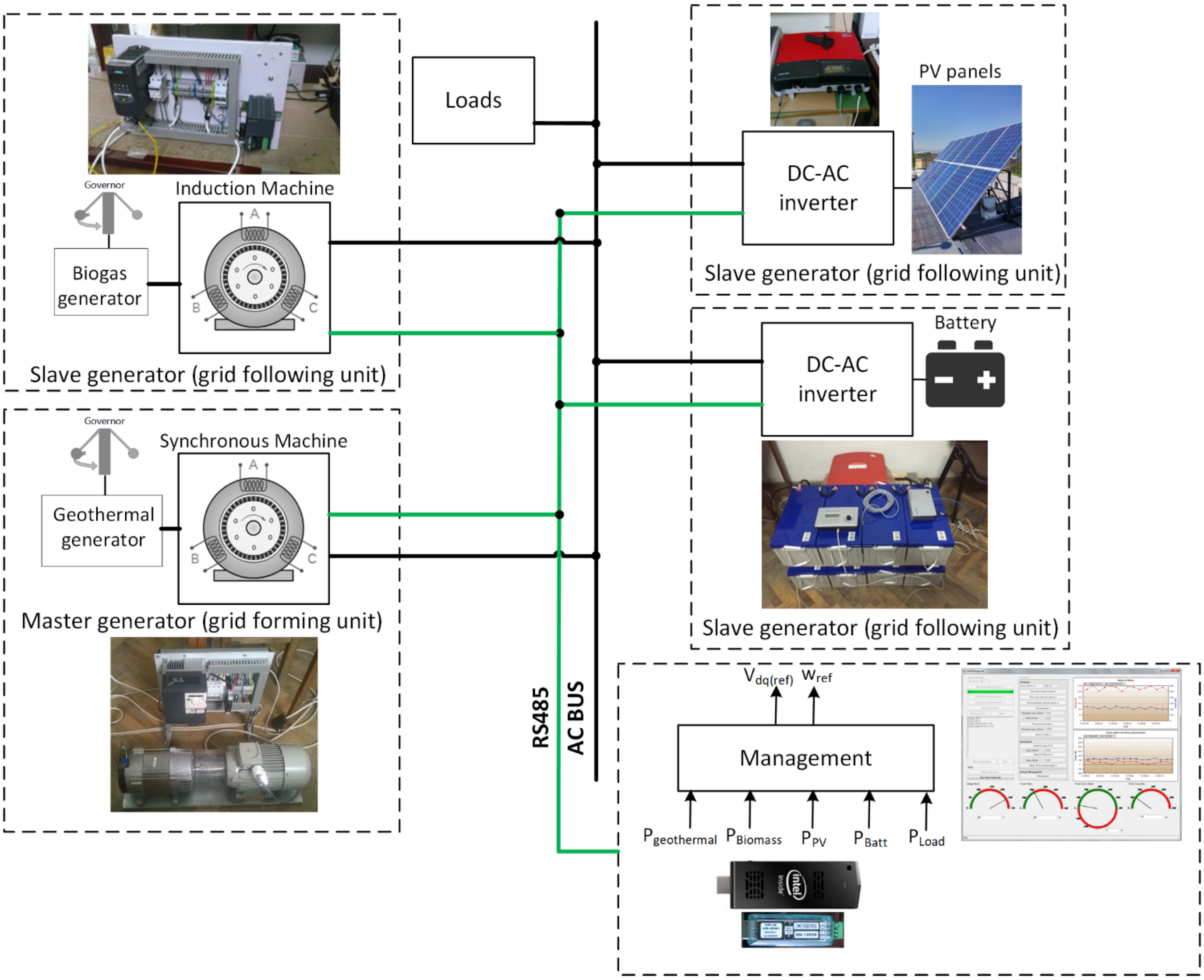

Fig. 1 Islanded renewable energy microgrid

As mentioned in [10], technical and economic analyses of HRES are of great importance for the efficient utilization of renewable energy resources. The design and optimization of a hybrid microgrid must consider the energy management strategy [11]. In [2], state-of-the-art optimization tools and techniques for HRES are reviewed. In [12] and [13], different optimization models, operating modes and objectives of renewable energy systems are presented. In [14], stochastic programming is used for energy scheduling in a microgrid. Wind and solar unpredictability and batteries management methods are presented in [15-17]. Optimal schedule in a microgrid is discussed in [18] for both islanded and grid-connected operation. Other methods such as mixed integer linear programming [19], prediction intervals [20] or load demand prediction [21] exist. Very few solutions presented in literature focus on actually building physical microgrids to study the concepts used for management algorithms or the optimization techniques. In [22] a fuzzy logic-based energy management system used in a residential microgrid is proposed looking to improve the life time of the batteries by maintaining the SOC close to 75%. As observed in [23–25] the simulated operation of microgrids is well-reported in literature but data analysis gathered from physically installed sites is neglected. No experimental tests are used to verify the ideal simulated models reported in [26–30]. Many studies e.g. [31] use mathematical models to test their works without using electrical simulation microgrid models. The lack of such simulations or physical models limit the impact of the results and many aspects are neglected. Few analyses made on installed and running microgrids can be mentioned but the percentage is insignificant when compared with the analyses made on simulated data. In [32] and [33], data gathered after installation and measured data for islanded PV systems respectively are presented. In [23], data from a hybrid microgrid installed in Kenya are acquired and the results can be generalized for hybrid solar/wind microgrids. The quantities are measured and available on MODBUS. In [24], an islanded hybrid solar/wind/fuel cell microgrid constructed on the Greek coast is used. Building such HRES microgrids with different combinations of renewable sources based on the specific location, as mentioned in [25], can also help the community by increasing job creation and not only zero emission energy production.

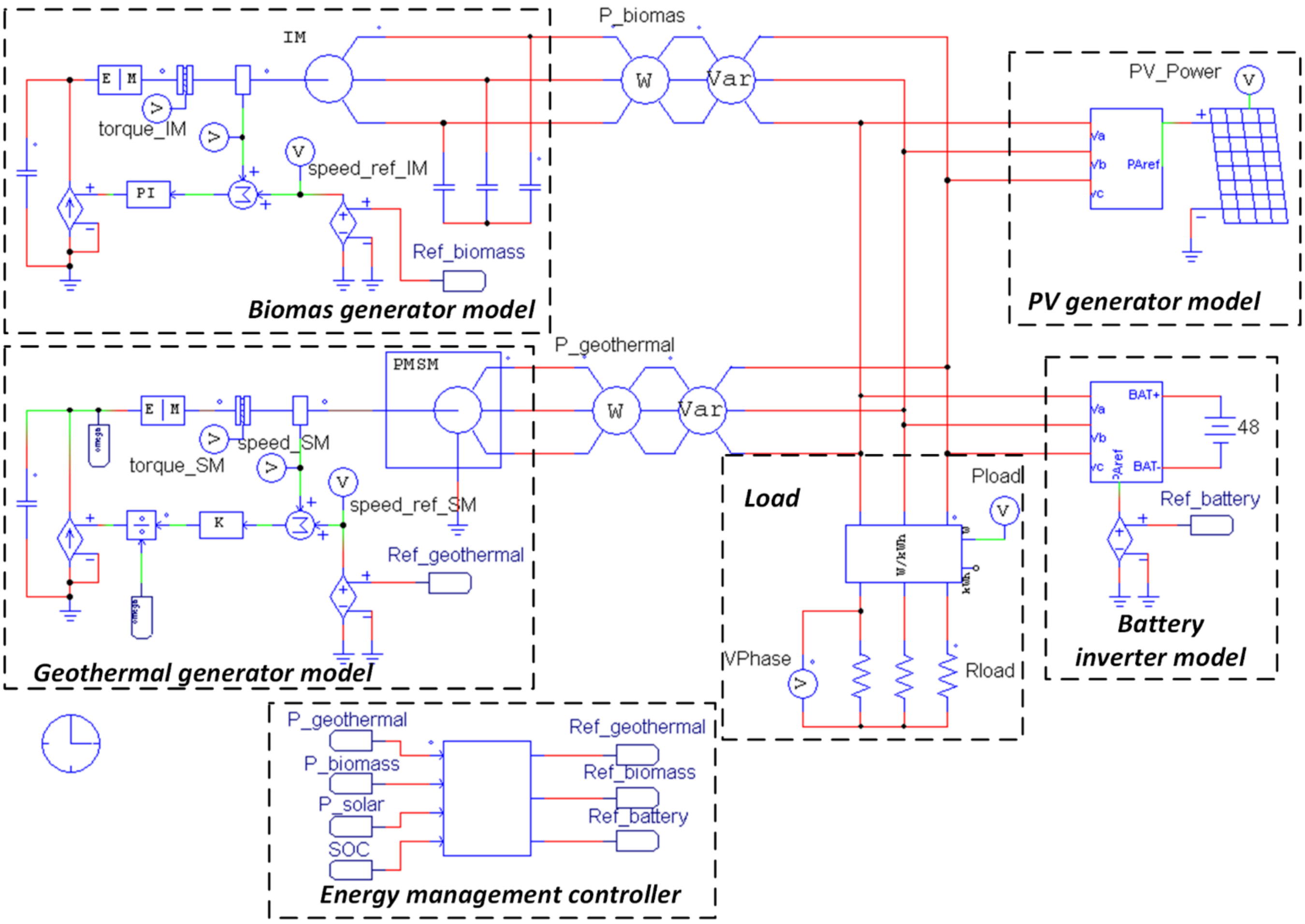

Fig. 2 Simulation model of the microgrid

In order to cover this lack of experimental data analysis, this paper proposes a HRES microgrid emulator built to test various management approaches when more than two generating units are used. The emulators are scalable and different scenarios for all types of renewable energy sources can be tested. In addition to the installed microgrid, an electrical simulation model that replicates the generators used in the actual HRES is developed, to test a range of energy management methods before applying them to the physical microgrid emulator. The simulation model can be adapted to any changes in the microgrid, for instance different droop characteristics of the generating units. Various control and energy management algorithms can be implemented and tested due to a communication network with Modbus and a central computing unit that gathers data and implements level two control methods.

The paper is structured as follows: Section II presents the microgrid emulator concept, Section III describes the electrical simulation model, whereas Section IV validates the simulation model with some case studies for the energy management algorithm. In section V, the experimental microgrid emulator is described. In section VI, the same case studies presented in section IV are applied to the experimental microgrid emulator and finally some conclusions are drawn in section VII.

2 THE MICROGRID EMULATOR CONCEPT

The proposed microgrid, illustrated in Fig.1, is based on three renewable energy sources and a two-level control management system. The first control level is implemented based on the droop characteristic of the electrical machines and the inverters used. The droop characteristics of the Sunny Island, SI, and Sunny Boy, SB, inverters are provided by the manufacturer in their data sheets. For the electrical machines employed, the droop characteristics were obtained experimentally. The renewable generators supply energy to the microgrid based on the availability of the resources. The primary resource is considered the geothermal energy since the geothermal water flow is considered constant. The Cycle-Charging algorithm is implemented as the second level energy management control method as an example but other control algorithms were also implemented. Hence, solar energy is used at its highest potential when available. The biogas resource is kept in reserve for peak load demands and critical moments, such as high discharge rates of the battery storage system. At transient moments and load power peaks the storage system will provide the necessary power in the microgrid. In order to maintain the stability in the microgrid, only one generator will act as a voltage source at one time and the rest of the generators will be current sources. When connected, the geothermal emulator is the master in the microgrid and sets the voltage level and frequency value. If the geothermal emulator is disconnected (equivalent with the geothermal resource not being available) the SI inverter will be the master in the microgrid. The voltage level and frequency values are set, and the inverter will use the batteries to keep the microgrid online until the geothermal resource will be available again. The grid forming inverter sets the voltage level and the frequency value in the microgrid.

The optimal system obtained during the design phase of the microgrid consists of a 2 kW geothermal generator, a 3kW biomass/biogas generator, 10 250 W PV panels and 12 VRLA 12 V 200 A/h batteries (Fig. 1). In order to validate the algorithm as proof of concept, a smaller scale microgrid is initially used. This features synchronous and asynchronous generators coupled to prime movers, whereas induction motors controlled by inverters are used to simulate the thermal machines.

3 THE MICROGRID SIMULATION MODEL

A simulation model for the microgid is developed and implemented using PSIM software [34] (Fig. 2). The model is used to test the interconnection of the generating units and the two-level management system.

As shown in Fig. 2, the microgrid system includes a model for the geothermal generating unit, one for the biomass generating unit and two inverter models, one for the PV array and the other one for the battery bank. The loads used in the proof of concept simulations are resistive ones. The control algorithms are based on ANSI-C and use a generic control block, shown as energy management controller (Fig. 2). The geothermal and biogas units are emulated by synchronous and induction electrical generators.

3.1 Geothermal generator unit simulation model

The geothermal generator unit is emulated by a synchronous generator, shown in Fig. 2. A model for the governor of the geothermal unit was also developed. A governor [35], is generally a device designed to maintain the shaft speed of a machine constant, as defined by an energy management system, regardless of the operating conditions. In this case, the governor is also used to implement the droop characteristic of the geothermal generator, as can be observed in Fig. 2. The variation of speed depending on the output power of the generator is described by eq. 1.

$$speed_{SM} = speed_{ref} - K_P \cdot P_{geothermal} \qquad \textit{eq. 1}$$

where $P_{geothermal}$ is the power generated by the geothermal unit, $speed_{ref}$ is the mechanical speed reference set by the management controller and $speed_{SM}$ represents the generator's measured speed (the process variable). K_P is the droop factor and based on its value the generated electrical power is proportional with the grid frequency. K_P can be obtained from eq. 2 and eq. 3:

$$\frac{(speed_{ref} - speed_{SM}) \cdot K}{\omega} = M = \frac{P_{geothermal}}{\omega} \qquad \textit{eq. 2}$$

$$K_P = 1/K \qquad \textit{eq. 3}$$

where M is the synchronous generator torque and ω is the mechanical angular frequency.

The simulation result for the synchronous machine droop characteristic is presented in Fig. 3 for the 49±1 Hz frequency domain, considering that the grid frequency, according to EU regulations, must not exceed nominal frequency (50 Hz in the present case) ±2 Hz.

`

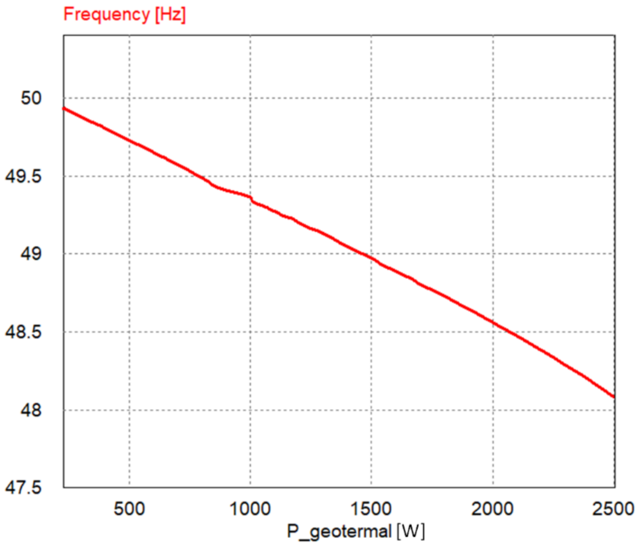

Fig. 3 Synchronous machine simulation droop characteristic for 49±1 Hz frequency domain.

Due to the fact that the controller is only a proportional type one, a steady state error is present, thus the proposed control method closely emulates the behaviour of the governor used to control the thermal machine.

3.2 Biomass generator unit simulation model

The biomass generator unit is emulated by an induction machine, IM, as shown in Fig. 2. The governor in this case uses a PI type controller. In this case the mechanical speed is constant and the generated power depends on the grid frequency due to the induction machine slip. The droop of the induction machine (Fig. 4) is obtained from the Kloss equation eq. 4.

$$M = \frac{2 \cdot M_K}{s_k/s + s/s_k} \qquad \textit{eq. 4}$$

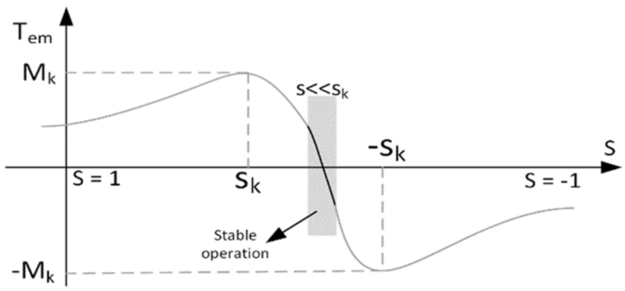

Fig. 4 Induction machine slip vs torque representation.

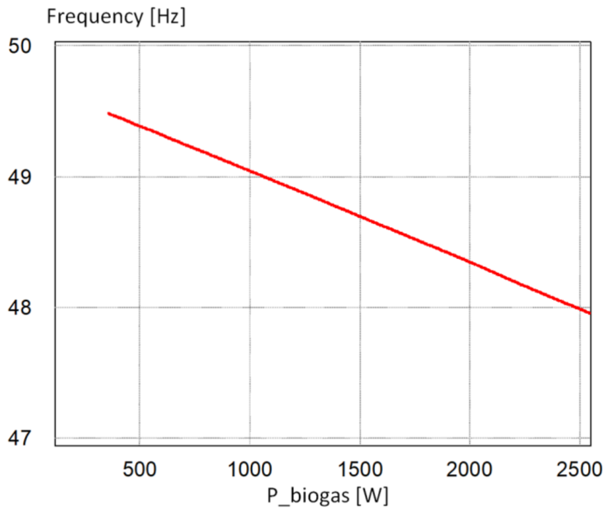

Fig. 5 Induction machine droop characteristic simulation for 49±1 Hz frequency domain

where M is the induction generator torque, M_K the breakdown torque, s the slip and s_k is the breakdown slip. Considering $s<<s_k$, eq. 5 is obtained.

$$M = \frac{2 \cdot M_K}{s_k} \cdot s \qquad eq.\ 5$$

Where

$$s = \frac{\omega_0 - \omega}{\omega_0} \qquad eq.\ 6$$

where ω is the angular frequency at rated speed and ω_0 is the no-load angular frequency.

$$\omega = \omega_0 - P \cdot K \qquad eq.\ 7$$

where K is the droop coefficient and can be calculated using the parameters of the generator (M_K and s_k).

$$K = \frac{s_k}{2 \cdot M_K} \qquad eq.\ 8$$

Fig. 5 illustrates the simulated linear dependency of power versus frequency for the 49±1 Hz variation domain.

3.3 Battery inverter simulation model

A bidirectional inverter connected to the grid on the AC side and to a battery bank on the DC side is simulated. The D-Q based control model is presented in Fig. 6. Based on the State of Charge (SOC) of the batteries, the load and the other generating units connected to the microgrid it will charge the batteries to a predefined set point or discharge the battery bank, supplying energy to the grid until a minimum state of charge set point is reached. The reference power of the inverter is set by the management controller in accordance to the loads and the power produced by the other microgrid generators. The battery bank model is composed of two parallel strings, each containing four 250 Ah batteries connected in series.

3.4 The PV inverter simulation model

A PV inverter is connected between the microgrid and a 2.8 kW PV array model. The PV inverter is also modelled using D-Q control Fig. 7. The following parameters are used for each solar panel in the PV array: 30.34 V MPP voltage, 8.24 A MPP current and a maximum output power of 250 W. The short circuit current of the panels is 8.24 A and the open circuit output voltage 37.4 V. The array has 12 panels connected in series, each made of 60 series connected cells and three bypass diodes. The I-V and P-V array characteristics are presented in Fig. 8.

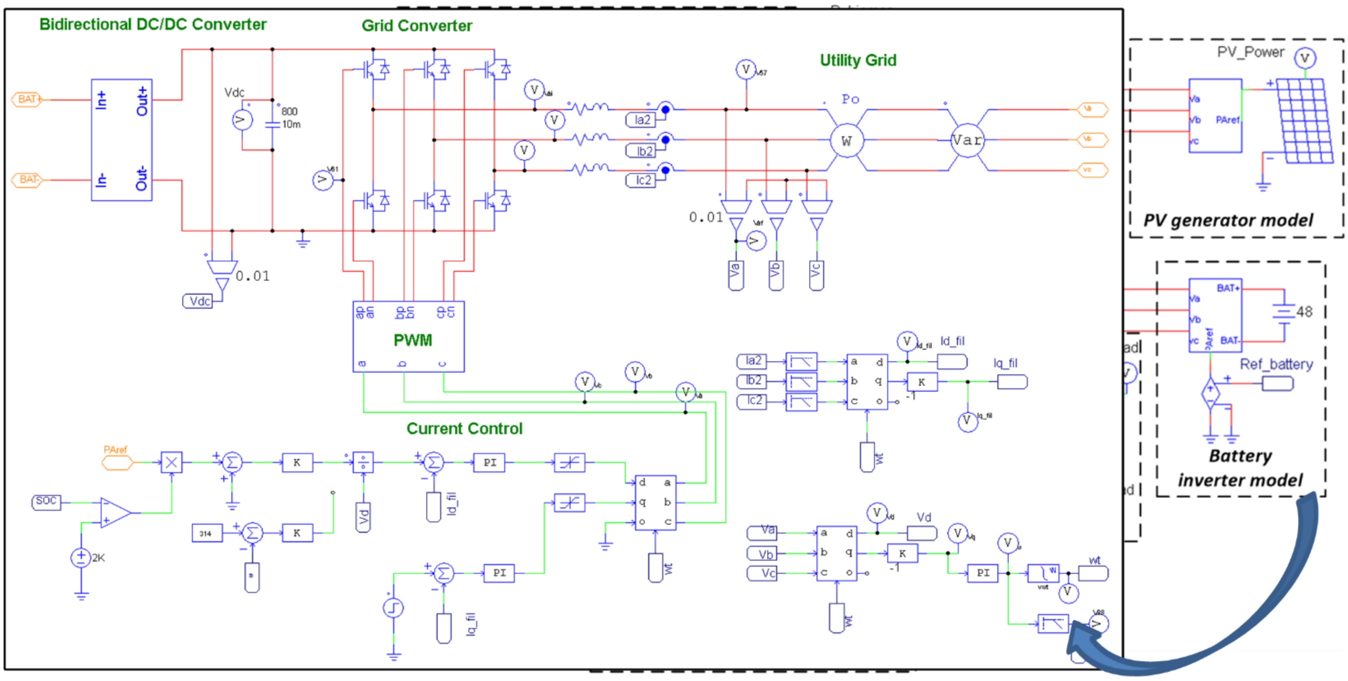

Fig. 6 Battery inverter schematic model

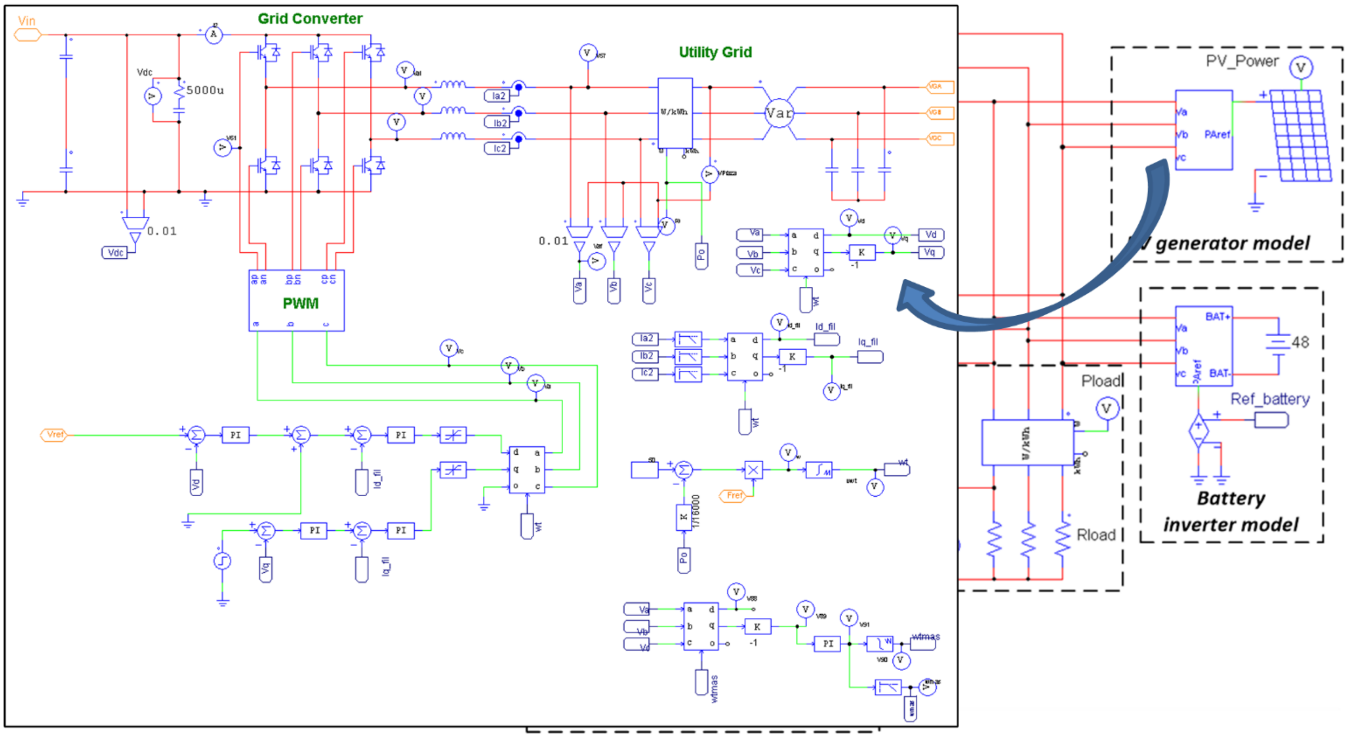

Fig. 7 PV inverter schematic model with droop control implemented.

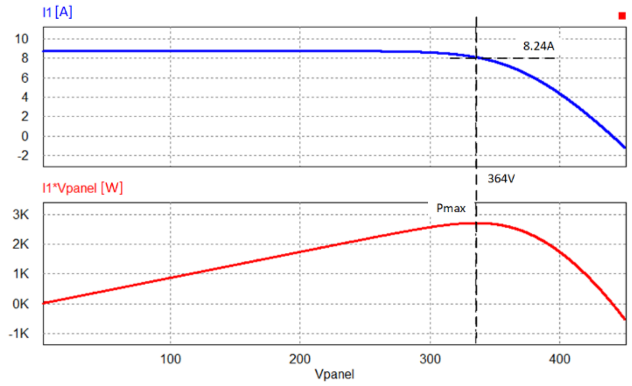

Fig. 8 I-V and P-V panels array characteristics.

The inverter uses the P&O [36] method to extract the maximum power from the PV array.

3.5 Energy management controller & control methods

The geothermal, biomass and solar power together with the state of charge of the batteries, are used by the controller to implement the secondary level control method by setting the power references of the generators. The management algorithm does not interfere with the PV inverter since it already uses a maximum Power Point Tracking (MPPT) algorithm to extract the maximum power form the PV array whenever the resource is available.

The management control method, written in C programming language, uses a hysteresis algorithm based on the battery's state of charge (SOC). The primary level control (droop) balances the power levels between the generating units at a steady state

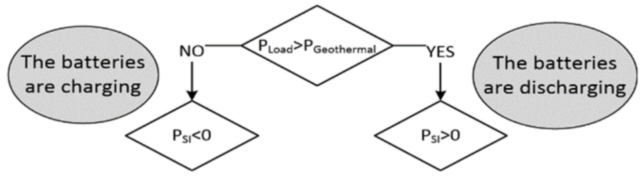

Fig. 9 Flowchart for simulation scenario 1.

point. After this point is reached, the secondary level algorithm makes the necessary adjustments to keep the SOC in the pre-set domain.

4 SIMULATION SCENARIOS – CASE STUDIES

Different scenarios [37] were simulated in order to validate the original models developed, as shown in Fig. 2.

4.1 Simulation scenario 1- geothermal generator & battery

A case study refers to power being delivered to the load when only the geothermal generator and the battery inverter are active in the microgrid. The flow chart (Fig. 9) and the results illustrated in Fig. 10 show how the battery inverter delivers microgrid power only when the demand is higher than the prescribed geothermal output power.

4.2 Simulation Scenario 2 - biomass generator added

Another presented case is when the biomass generator is connected to the grid and running Fig. 11 and Fig. 12.

4.3 Simulation Scenario 3 - PV energy added

Whenever the PV panels produce energy, the power delivered to the microgrid by the PV inverter depends on the irradiance. As presented in Fig. 13, the biomass generator will be used in order to compensate for the variations of the

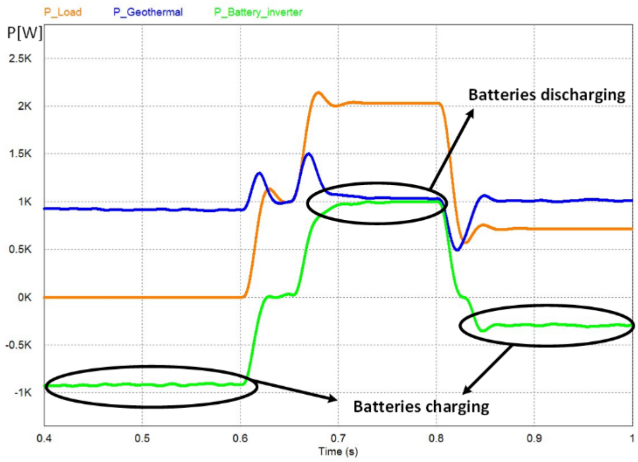

Fig. 10 Simulation results for Scenario 1 - microgrid with only geothermal generator and batteries inverter

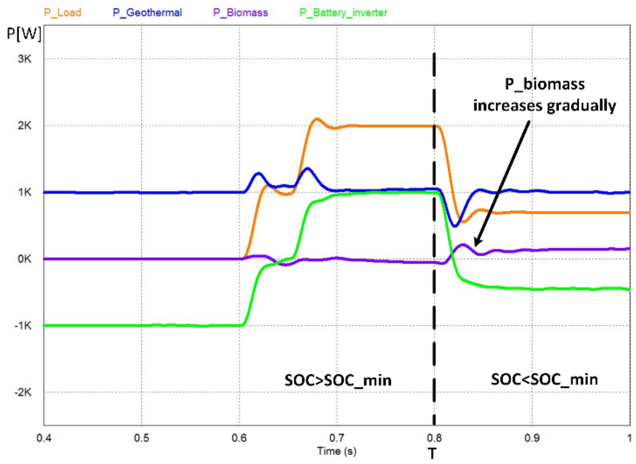

Fig. 11 Simulation results for Scenario 2, when the biomass generator is connected to the microgrid.

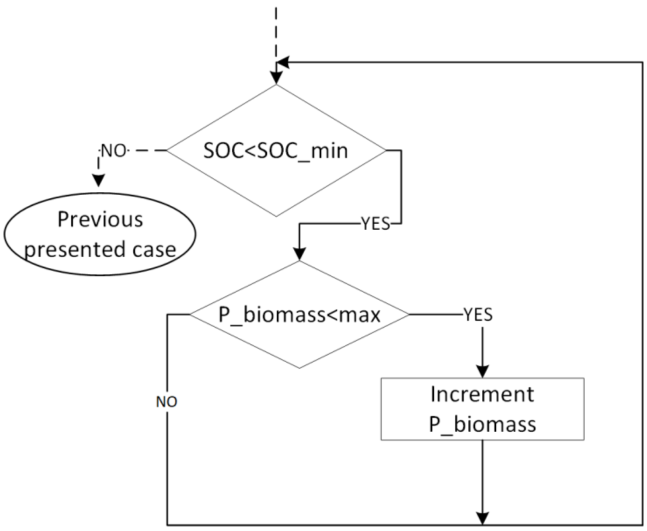

Fig. 12 Flowchart for the simulation scenario 2.

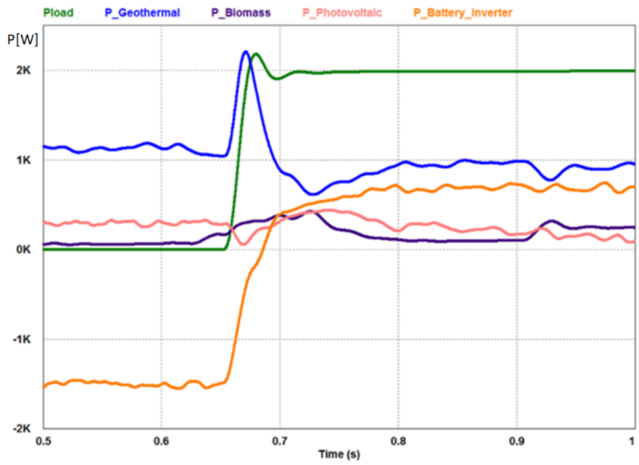

Fig. 13 Simulation results when solar energy is available.

solar irradiance and keep the SOC in the pre-established limits for the cycle charging management method.

The battery inverter and geothermal generator will have the same behaviour as in the previously presented cases. The power delivered by the PV inverter is not fed back to the management controller since the purpose of using the cycle charging method is to take advantage as much as possible of the solar resource. When available, the energy can be used to deliver power to the loads or to charge the batteries. The maximum SOC limit imposed by the algorithm can be exceeded only by the PV resource. If the SOC will reach its maximum physical value, the PV inverter will reduce its output power to 0W. The difference between the physical maximum SOC and the one imposed by the algorithm can be considered an energy buffer for the power produced by the PV array.

4.4 Simulation Scenario Case Study 4 – all sources except PV connected, operating under various regimes

A scenario including multiple aspects of the microgrid working in different situations is shown in Fig. 14. Since the control method does not interfere with the PV energy flow and level, as mentioned before, the scenario does not include this resource. In terms of real life experimental results, this is the case study for very cloudy weather.

The time intervals (A-E) refer to different modes of the microgrid operation. During interval A, the geothermal generator produces almost the entire amount of power demanded by the load and the batteries' rate of discharge is insignificant. During interval B, as it can be seen on the SOC waveform, the batteries are charging. The energy is delivered by the geothermal generator. When the SOC reaches SOC_max in interval C, the control methods will prevent the geothermal generator from delivering power in the microgrid and charging the batteries. The purpose of the cycle charging is to keep the SOC between the two pre-set limits. If the load power demand increases, during interval D, the power is delivered by the battery inverter and the SOC starts to decrease. When the SOC reaches SOC_min during interval E, the geothermal generator is brought out of the IDLE state and will deliver power to the microgrid.

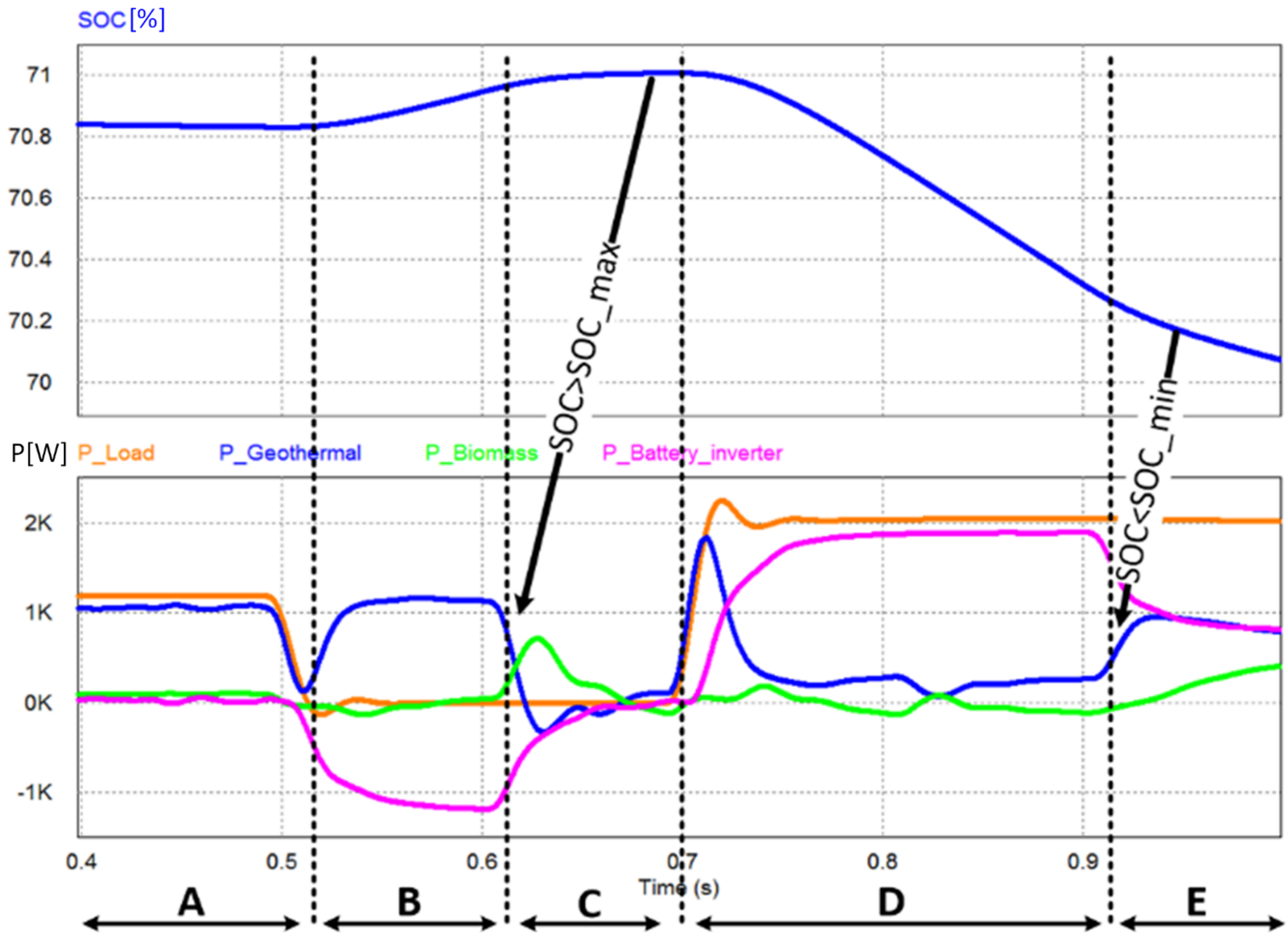

Fig. 14 Simulation results for a cloudy day Scenario 4.

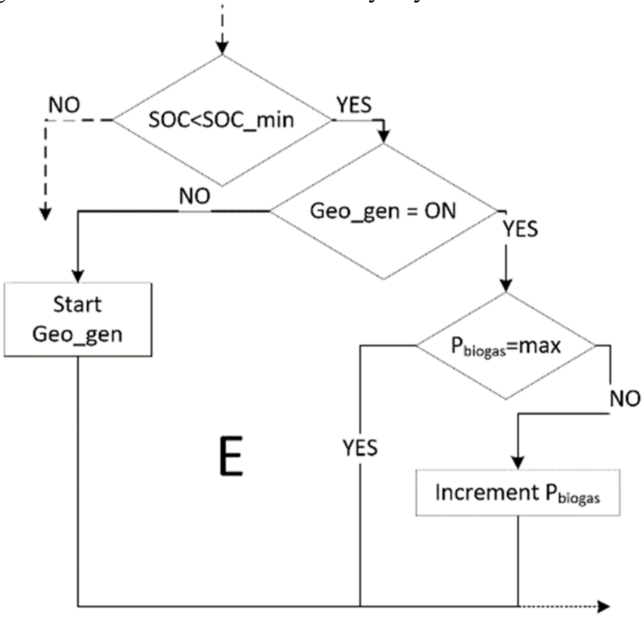

Fig. 15 Flow chart for the E interval in Fig. 14.

If the batteries are still discharging, the biomass generator is also brought out of the IDLE state and will gradually increase the power delivered to the microgrid.

Fig. 15 illustrates the flowchart part corresponding to interval E from Fig. 14. The presented model of the microgrid works for both cases: the primary level control (droop control) and the secondary level control (cycle charge method).

5 THE MICROGRID EXPERIMENTAL MODEL

An experimental microgid is implemented in the laboratory. The microgrid is used to validate the model through experimental results, to test the interconnection of different types of generating units and to perform a real-life test for the two-level management methods. The microgrid is composed of a geothermal emulator, a biomass emulator, a photovoltaic generator and a storage system.

5.1 The battery inverter and storage

The battery inverter used in the experimental microgrid is an inverter from SMA, Sunny Island 6.0H, rated at 4.5 kW. The inverter charges a battery bank composed of 2 parallel strings of batteries. Each string contains four 200 Ah VRLA batteries connected in series. The inverter used takes into account the depth of discharge and the aging of the battery bank. The input port of this inverter is used to connect the geothermal generator emulator. Thus, when the geothermal unit is OFF, the battery inverter acts as the master unit providing the grid voltage and frequency.

Fig. 16 Storage system.

This inverter becomes a slave unit when the geothermal generator turns ON. In this case, the master unit is the geothermal generator, which sets the grid voltage and frequency. All the other inverts and generators work in synchronism with the geothermal unit. The storage system is depicted in Fig. 16.

5.2 The solar inverter and PV array

The solar inverter is a Sunny Boy SB3600-TL, rated at 3.8 kW. This inverter is used to extract the maximum power point (MPP) from the solar panels and to inject it in the microgrid. This inverter works as a slave unit. The PV array is composed of twelve solar panels from ET-Solar, rated at 250 W each.

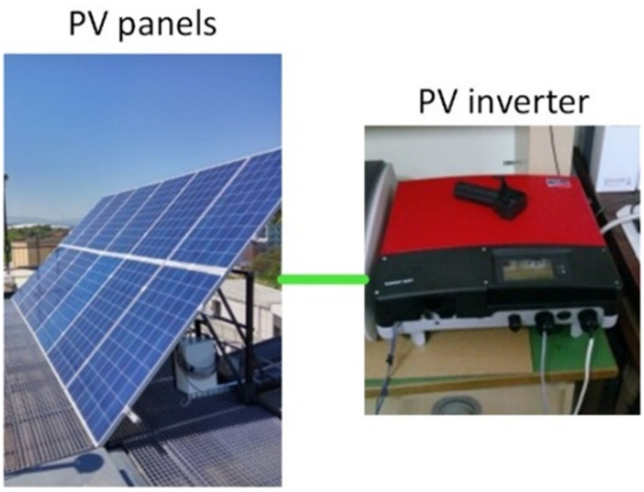

Fig. 17 Photovoltaic system.

All the modules are connected in series to match the input voltage of the solar inverter, 125 V-500 V. The MPP current and voltage of a solar panel is 8.24 A and 30.34 V, respectively. The orientation of the panels is 137° with -43° azimuth and an inclination of 44° from horizontal line. The photovoltaic generator is pictured in Fig. 17.

5.3 The emulator for the geothermal generator

The geothermal generator is composed of a synchronous machine driven by an inverter controlled induction motor. The method used to control the motor is constant U/f. The error in the speed of the U/f method and the slip of the induction machine are used to emulate the geothermal generator droop characteristic. The set-point for the base frequency is set by the management algorithm through Modbus.

The geothermal emulator droop characteristic obtained experimentally is represented in Fig. 18. A droop factor of $8 \cdot 10^{-4}$ shows the dependency of the grid frequency with the output power. The geothermal emulator is pictured in Fig. 19.

5.4 The emulator for the biogas generator

The same principle is used to build the biogas emulator. An induction motor controlled by an inverter is used to drive an induction generator. In this case, vector control is used in the inverter and the slip frequency of the induction machine gives the droop characteristic of the biomass generator.

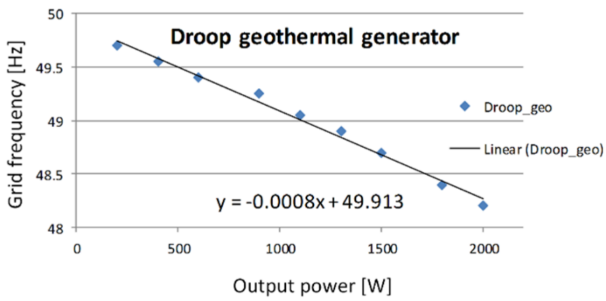

Fig. 18 Geothermal generator droop characteristic.

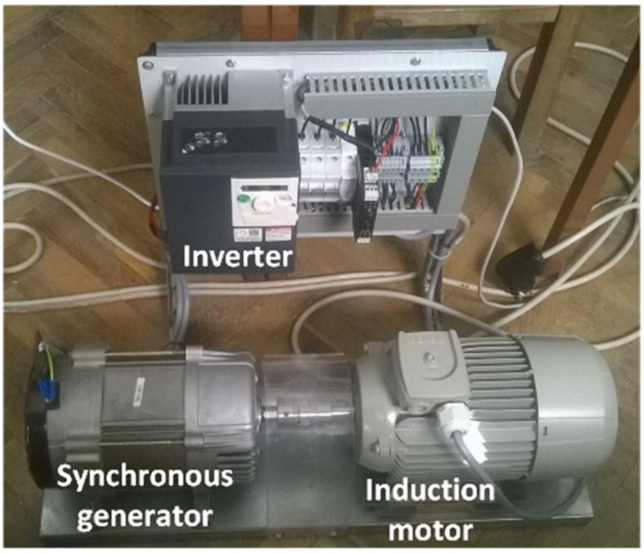

Fig. 19 Geothermal emulator.

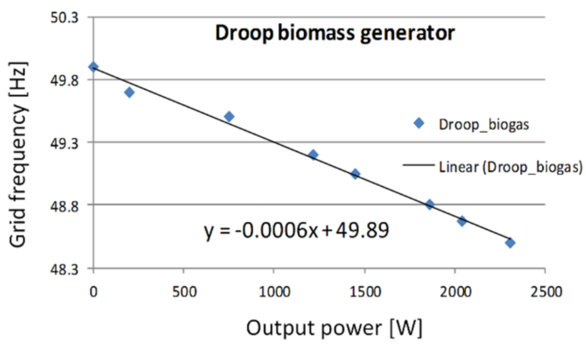

Fig. 20 Biomass emulator droop characteristic.

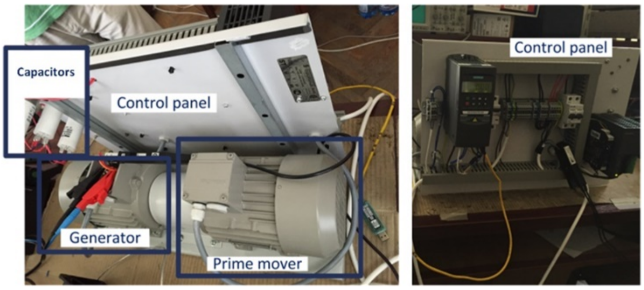

Fig. 21 Biomass emulator.

The set-point for the base frequency is set by the management algorithm through Modbus.
The measured droop characteristic for the biomass emulator is represented in Fig. 20. It can be seen that the droop factor is $6 \cdot 10^{-4}$. The biomass emulator is pictured in Fig. 21.

5.5 Auxiliary equipment and communication

A method to send the commands to the microgrid and to measure the process variables from the microgrid is needed for the control algorithm based on battery cycle charging implementation. A bidirectional three wire RS485 serial communication network is built for this purpose. The communication protocol used in the network uses Modbus compatible data frameworks but is also compatible with the data protocols used by the inverters. Beside the communication modules needed by the inverters, there is a need for other equipment in order to give the geothermal and biomass emulators communication capabilities. The command signals are fed to the emulators through Modbus to analog converters and Modbus output compatible power meters are used for the electrical measurement. The network communication master is the central computing unit. The program that implements the master's communication functions and the cycle charging battery management algorithm is written in ANSI C, thus being highly portable. The physical interface between the network and the master is made by an USB to RS-485 interface. The connections of the equipment are presented in Fig. 22. The set points for the SMA equipment are directly sent through the communication network, but the emulators need Modbus to analog transducers for their commands.

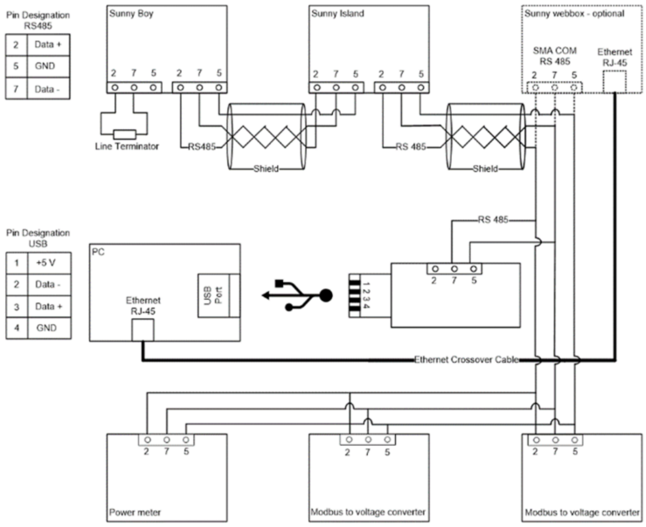

Fig. 22 The microgrid communication network.

6 EXPERIMENTAL RESULTS AND DISCUSSION

The scenarios used with the simulation model represented in Fig. 2, based on which the results presented in section IV were obtained, are tested in the experimentally implemented microgrid.

In the first scenario (Fig. 23), the photovoltaic resource is not available and the biomass one is deactivated to see how the geothermal emulator and battery inverter work together when connected in parallel. Initially, the power generated by the geothermal emulator is used to charge the batteries. If a resistive load of 1 kW is connected, the charging power decreases nearly to zero and the load power demand is fully provided by the geothermal generator.

If the load increases by 1 kW, the battery inverter will deliver power in the microgrid and compensate for the lack of power. The energy flow changes and the batteries start to discharge. The geothermal emulator power was limited through the management controller to 1 kW. The microgrid measured values are sampled each minute and the sample number is presented on the x axis. After the 2 kW load is disconnected from the microgrid and a 750 W load is connected, the 250 W difference between the geothermal maximum power delivered in the microgrid and load is fed into the batteries, charging them.

The difference in the second scenario (Fig. 24) is that the SOC falls below the SOCmin value imposed by the battery cycle control method. In this case, the biomass generator is connected to the microgrid, but it will not deliver power in the microgrid until the SOC is smaller than SOCmin.

From the load point of view, 4 cases can be observed: 1- the load is disconnected from the microgrid and the power generated by the geothermal unit is transferred to the batteries; 2- if a 1 kW load is connected to the microgrid, the power is delivered by the geothermal generator; 3- a second 1 kW load is connected in parallel with the first load and the batteries inverter will deliver power. The batteries will start to discharge; 4- The 1 kW loads are disconnected and a 750 W load takes their place.

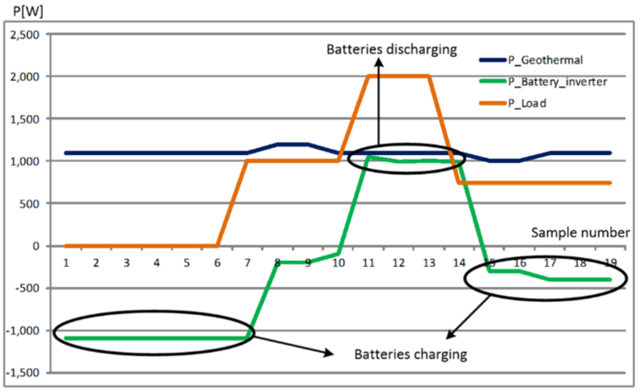

Fig. 23 Experimental results for the first scenario.

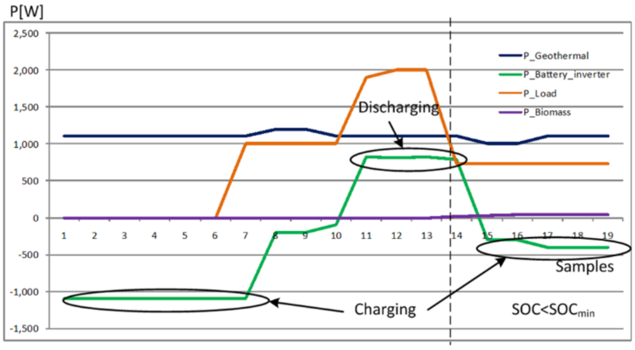

Fig. 24 Experimental results for the second scenario.

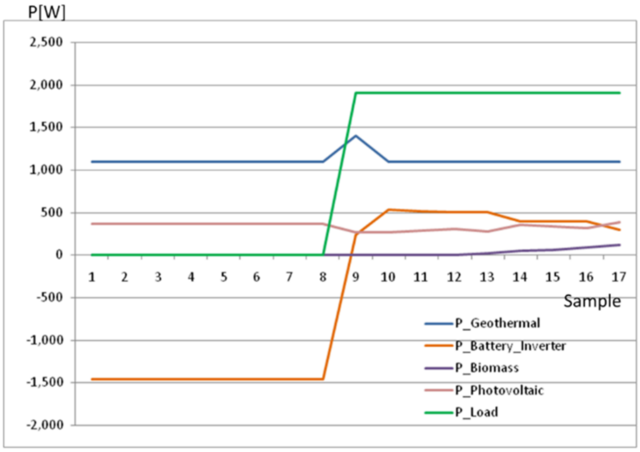

Fig. 25 Experimental results for the third scenario.

The load demand is provided by the geothermal generator while the biomass power is gradually increased if the SOC reaches the minimum imposed value.

The management algorithm was designed in such a way that if the SOC is smaller than SOC_{min} the microgrid generators must bring the SOC value over the minimum value in the shortest amount of time possible, no matter what the load variations are. As one can see, the batteries are charging on the right side of Fig. 24.

In the third scenario (Fig. 25), the geothermal, biomass and battery inverter work as in the cases previously presented. The difference now is that the photovoltaic resource is present. The power produced by the biomass generator counteracts the luminosity variations.

In the fourth presented scenario, the case when the SOC is greater than the one imposed by the cycle charging algorithm is highlighted. When SOC is greater than SOC_{max}, the geothermal generator will not deliver power anymore in the microgrid and in case a load is connected, the battery inverter will deliver the power needed. The batteries will start discharging and until the SOC value is between SOC_{min} and SOC_{max}, only the battery inverter will deliver power in the microgrid if the photovoltaic resource is not available (Fig. 26). If the photovoltaic resource is available, based on the power it produces, the whole power needed by the load or a part of it will be supplied by it. In case P_{Load} is smaller than $P_{Photovoltaic}$, the batteries will charge with the excess power. The biomass generator is controlled by the management controller and will produce power to counteract the irradiance variations. The purpose of the management control method is to maintain the SOC between the two imposed limits and to keep the power of the battery inverter to zero to the extent possible.

7 CONCLUSIONS

Through this paper, the authors cover the lack of literature regarding experimental hybrid renewable energy microgrids setups. Even though there are several other works in the literature that simulate/emulate the operation of a microgrid we consider the three renewable energy sources combination (solar, geothermal and biomass) as being original. Furthermore, the thermal machines that drive the electrical generators are replaced by asynchronous electrical machines with vector control for the synchronous generator on one hand to cancel the slip and with scalar control for the induction generator on the other hand. In the scalar control case the droop control is emulated through the slip of the induction machine.

Besides the implemented experimental microgrid a complex simulation model in PSIM software with a structure that replicates the equipment has been proposed and built. The results obtained during the simulation phase are very close to the emulated ones as one can see analysing the results provided. Compared with other very complex emulators the proposed one is relative cheap and can be used for different running scenarios and control methods. The proposed microgrid and the corresponding simulation schematic can be used as a hardware in the loop system to test energy management algorithms and as a microgrid emulator to test various microgrid configurations with respect to a range of renewable energy sources.

The proposed hybrid energy microgrid, in this configuration, is recommended for a practical case of a greenhouse situated in an area where geothermal resources can be found. As one can see, the primary energy sources used by the energy management algorithm are geothermal and biogas, with the more expensive fuel being used only for the critical cases of high energy need. The management algorithm uses the cycle charge method since the solar (PV) energy is the least expensive when comparing the fuel costs and from an economical point of view it is better to use it rather than the biogas fuels. Because of the variety of renewable energy sources available in the proposed microgrid, the power demand of a greenhouse can be sustained even in worst-case scenarios, if the generators'

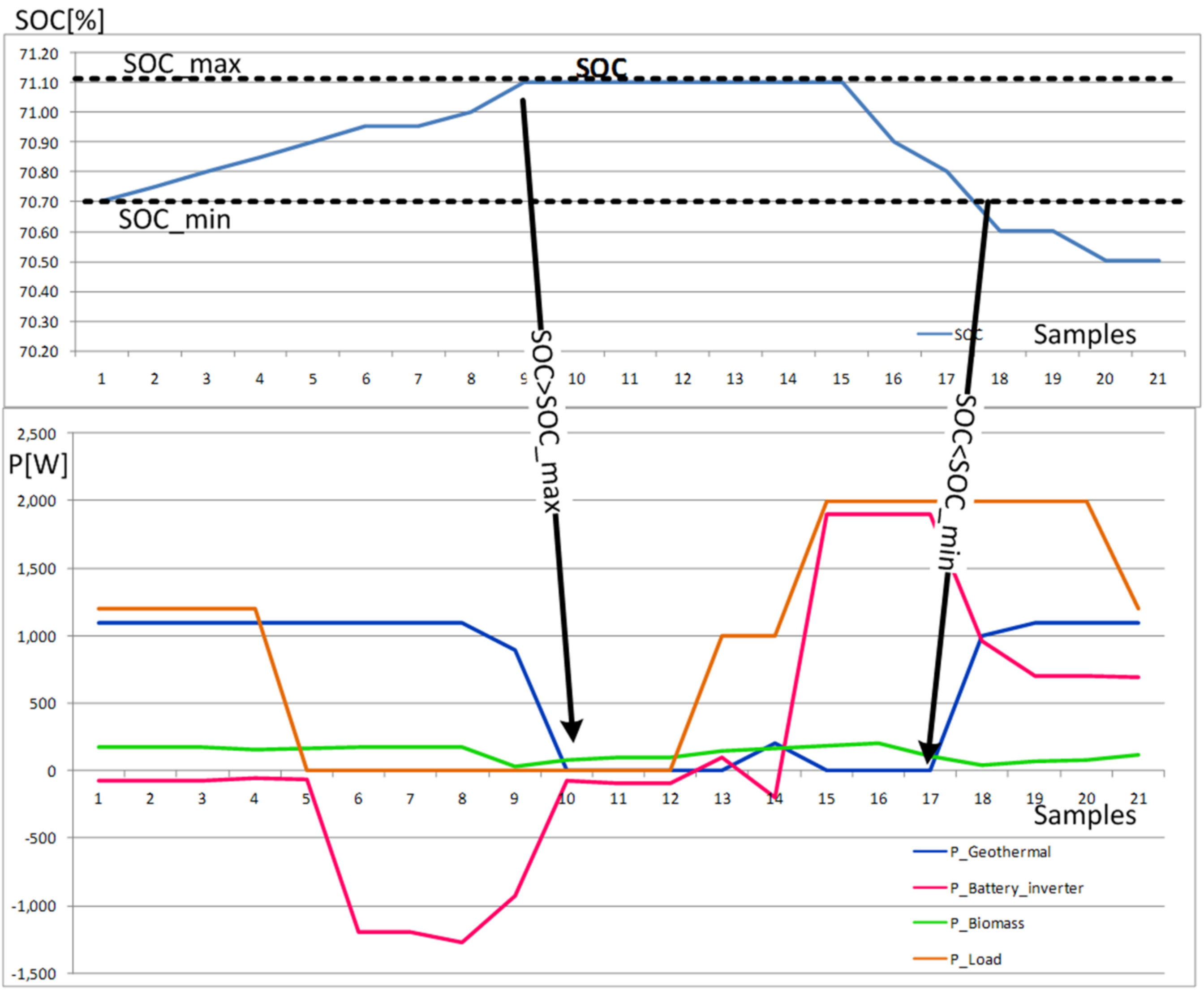

Fig. 26 Experimental results for the fourth scenario.

rated power is appropriately chosen and the storage bank is correctly designed.

For further development the irradiance at the PV installation site will be collected in near future. The proposed microgrid, in conjunction with the original energy management algorithm presented in the paper, can offer high efficiency when correlated with meteorological data and with fuel and maintenance data costs, thus becoming a predictive and cost-effective algorithm. Using meteorological data such as the solar irradiance a load scheduler can be built thus reducing the running time and cost of the biomass generator for example. The batteries SOC minimum and maximum values used by the management method can be updated in real time based on these values.

The microgrid uses a two-level control structure: the primary level, where each generating unit controls its output power based on its droop characteristic, and the secondary control level, implemented by the energy management control unit. Along with this primary level control based on droop, for the secondary level different type of algorithms can be implemented by introducing cost function for optimization.

The simulation and microgrid are scalable and thus the test results obtained are generally valid for a hybrid configuration type. Cost effectiveness and optimization analysis can therefore be further implemented for HRES.

ACKNOWLEDGMENT

This paper is supported through the programme "Partnerships in priority domains - PNII", by MEN - UEFISCDI, project no. 53/01.07.2014.

REFERENCES

[1] Rahman S. Economic impact of integrating photovoltaics with conventional electric utility operation. IEEE Trans Energy Convers 1990;5:422–8. doi:10.1109/60.105264.

[2] Fathima AH, Palanisamy K. Optimization in microgrids with hybrid energy systems – A review. Renew

Sustain Energy Rev 2015;45:431–46. doi:10.1016/j.rser.2015.01.059.

[3] Dagdougui H, Minciardi R, Ouammi A, Robba M, Sacile R. A Dynamic Decision Model for the Real-Time Control of Hybrid Renewable Energy Production Systems. IEEE Syst J 2010;4:323–33. doi:10.1109/JSYST.2010.2059150.

[4] Hemmati M, Amjady N, Ehsan M. System modeling and optimization for islanded micro-grid using multi-cross learning-based chaotic differential evolution algorithm. Int J Electr Power Energy Syst 2014;56:349–60. doi:10.1016/j.ijepes.2013.11.015.

[5] Hajizadeh A, Golkar MA. Intelligent power management strategy of hybrid distributed generation system. Int J Electr Power Energy Syst 2007;29:783–95. doi:10.1016/j.ijepes.2007.06.025.

[6] Dasgupta S, Mohan SN, Sahoo SK, Panda SK. A Plug and Play Operational Approach for Implementation of an Autonomous-Micro-Grid System. IEEE Trans Ind Informatics 2012;8:615–29. doi:10.1109/TII.2012.2193893.

[7] Chen C, Duan S, Cai T, Liu B, Hu G. Smart energy management system for optimal microgrid economic operation. IET Renew Power Gener 2011;5:258. doi:10.1049/iet-rpg.2010.0052.

[8] Nehrir MH, Wang C, Strunz K, Aki H, Ramakumar R, Bing J, et al. A Review of Hybrid Renewable/Alternative Energy Systems for Electric Power Generation: Configurations, Control, and Applications. IEEE Trans Sustain Energy 2011;2:392–403. doi:10.1109/TSTE.2011.2157540.

[9] Liang H, Zhuang W. Stochastic Modeling and Optimization in a Microgrid: A Survey. Energies 2014;7:2027–50. doi:10.3390/en7042027.

[10] Jung J, Villaran M. Optimal planning and design of hybrid renewable energy systems for microgrids. Renew Sustain Energy Rev 2017;75:180–91. doi:10.1016/J.RSER.2016.10.061.

[11] Ramli MAM, Bouchekara HREH, Alghamdi AS. Optimal sizing of PV/wind/diesel hybrid microgrid system using multi-objective self-adaptive differential evolution algorithm. Renew Energy 2018;121:400–11. doi:10.1016/J.RENENE.2018.01.058.

[12] Iqbal M, Azam M, Naeem M, Khwaja AS, Anpalagan A. Optimization classification, algorithms and tools for renewable energy: A review. Renew Sustain Energy Rev 2014;39:640–54. doi:10.1016/J.RSER.2014.07.120.

[13] Kerdphol T, Fuji K, Mitani Y, Watanabe M, Qudaih Y. Optimization of a battery energy storage system using particle swarm optimization for stand-alone microgrids. Int J Electr Power Energy Syst 2016;81:32–9. doi:10.1016/J.IJEPES.2016.02.006.

[14] Su W, Wang J, Roh J. Stochastic Energy Scheduling in Microgrids With Intermittent Renewable Energy Resources. IEEE Trans Smart Grid 2014;5:1876–83. doi:10.1109/TSG.2013.2280645.

[15] Mohammadi S, Mozafari B, Solimani S, Niknam T. An Adaptive Modified Firefly Optimisation Algorithm based on Hong's Point Estimate Method to optimal operation management in a microgrid with consideration of uncertainties. Energy 2013;51:339–48. doi:10.1016/J.ENERGY.2012.12.013.

[16] Baziar A, Kavousi-Fard A. Considering uncertainty in the optimal energy management of renewable micro-grids including storage devices. Renew Energy 2013;59:158–66. doi:10.1016/J.RENENE.2013.03.026.

[17] Pascual J, Barricarte J, Sanchis P, Marroyo L. Energy management strategy for a renewable-based residential microgrid with generation and demand forecasting. Appl Energy 2015;158:12–25. doi:10.1016/J.APENERGY.2015.08.040.

[18] Gupta RA, Gupta NK. A robust optimization based approach for microgrid operation in deregulated environment. Energy Convers Manag 2015;93:121–31. doi:10.1016/J.ENCONMAN.2015.01.008.

[19] Hosseinzadeh M, Salmasi FR. Robust Optimal Power Management System for a Hybrid AC/DC Micro-Grid. IEEE Trans Sustain Energy 2015;6:675–87. doi:10.1109/TSTE.2015.2405935.

[20] Kuznetsova E, Ruiz C, Li Y-F, Zio E. Analysis of robust optimization for decentralized microgrid energy management under uncertainty. Int J Electr Power Energy Syst 2015;64:815–32. doi:10.1016/J.IJEPES.2014.07.064.

[21] Hussain A, Bui V-H, Kim H-M. Robust Optimization-Based Scheduling of Multi-Microgrids Considering Uncertainties. Energies 2016;9:278. doi:10.3390/en9040278.

[22] Arcos-Aviles D, Pascual J, Guinjoan F, Marroyo L, Sanchis P, Marietta MP. Low complexity energy management strategy for grid profile smoothing of a residential grid-connected microgrid using generation and demand forecasting. Appl Energy 2017;205:69–84. doi:10.1016/J.APENERGY.2017.07.123.

[23] Louie H. Operational analysis of hybrid solar/wind microgrids using measured data. Energy Sustain Dev 2016;31:108–17. doi:10.1016/J.ESD.2016.01.003.

[24] Fathabadi H. Novel standalone hybrid solar/wind/fuel cell power generation system for remote areas. Sol Energy 2017;146:30–43. doi:10.1016/J.SOLENER.2017.01.071.

[25] Hosseinimehr T, Ghosh A, Shahnia F. Cooperative control of battery energy storage systems in microgrids. Int J Electr Power Energy Syst 2017;87:109–20. doi:10.1016/j.ijepes.2016.12.003.

[26] Singh S, Agarwal S, Tiwari GN, Chauhan D. Application of genetic algorithm with multi-objective function to improve the efficiency of glazed photovoltaic thermal system for New Delhi (India) climatic condition. Sol Energy 2015;117:153–66. doi:10.1016/J.SOLENER.2015.04.025.

[27] Singh S, Agrawal S, Avasthi DV. Design, modeling and performance analysis of dual channel semitransparent photovoltaic thermal hybrid module in the cold environment. Energy Convers Manag 2016;114:241–50. doi:10.1016/J.ENCONMAN.2016.02.023.

[28] Kabalci E. Design and analysis of a hybrid renewable energy plant with solar and wind power. Energy

Convers Manag 2013;72:51–9. doi:10.1016/J.ENCONMAN.2012.08.027.

[29] Mahmoud MS, Alyazidi NM, Abouheaf MI. Adaptive intelligent techniques for microgrid control systems: A survey. Int J Electr Power Energy Syst 2017;90:292–305. doi:10.1016/J.IJEPES.2017.02.008.

[30] Majumder R, Bag G. Parallel operation of converter interfaced multiple microgrids. Int J Electr Power Energy Syst 2014;55:486–96. doi:10.1016/J.IJEPES.2013.09.008.

[31] Craparo E, Karatas M, Singham DI. A robust optimization approach to hybrid microgrid operation using ensemble weather forecasts. Appl Energy 2017;201:135–47. doi:10.1016/J.APENERGY.2017.05.068.

[32] Tamir K, Urmee T, Pryor T. Issues of small scale renewable energy systems installed in rural Soum centres in Mongolia. Energy Sustain Dev 2015;27:1–9. doi:10.1016/J.ESD.2015.04.002.

[33] Díaz P, Peña R, Muñoz J, Arias CA, Sandoval D. Field analysis of solar PV-based collective systems for rural electrification. Energy 2011;36:2509–16. doi:10.1016/J.ENERGY.2011.01.043.

[34] PSIM User Manual, Powersim Inc., 2017. [Online]. Available:https://powersimtech.com/drive/uploads/2017/11/PSIM-User-Manual.pdf

[35] Dengler P, Geimer M, Zahoransky R. Potential of Reduced Fuel Consumption of Diesel-Electric APUs at Variable Speed in Mobile Applications, 2011. doi:10.4271/2011-24-0075.

[36] Ali AIM, Sayed MA, Mohamed EEM. Modified efficient perturb and observe maximum power point tracking technique for grid-tied PV system. Int J Electr Power Energy Syst 2018;99:192–202. doi:10.1016/J.IJEPES.2017.12.029.

[37] Radu E, Dorin P, Toma P, Eniko L. An islanded renewable energy microgrid emulator for geothermal, biogas, photovoltaic and lead acid battery storage. 2017 IEEE 26th Int. Symp. Ind. Electron., IEEE; 2017, p. 2109–14. doi:10.1109/ISIE.2017.8001583.